Competing interactions in ferromagnetic/antiferromagnetic perovskite superlattices

Y. Takamura[1], F. Yang[1], and N. Kemik[1], E. Arenholz[2], M.B. Biegalski[3], and H.M. Christen[3]

[1]Department of Chemical Engineering and Materials Science, UC Davis, CA 95616

[2]Advanced Light Source, Lawrence Berkeley National Laboratory, Berkeley, CA 94720

[3]Center for Nanophase Materials Science, Oak Ridge National Laboratory, Oak Ridge, TN 37831

Receipt Date:

Abstract

Soft x-ray magnetic dichroism, magnetization, and magnetotransport measurements demonstrate that the competition between different magnetic interactions (exchange coupling, electronic reconstruction, and long-range interactions) in $La_{0.7}Sr_{0.3}FeO_3$ (LSFO) / $La_{0.7}Sr_{0.3}MnO_3$ (LSMO) perovskite oxide superlattices leads to unexpected functional properties. The antiferromagnetic order parameter in LSFO and ferromagnetic order parameter in LSMO show a dissimilar dependence on sublayer thickness and temperature, illustrating the high degree of tunability in these artificially-layered materials.

PACS numbers: 75.70.Cn, 78.70.Dm, 75.47.Gk

Complex materials with multiple order parameters hold the promise to yield systems with highly-tunable and stimulus-sensitive properties as required for sensing, energy conversion, and information technology applications. However, the competition between multiple order parameters places a great challenge on our ability to predict the resulting physical properties and thus to create complex materials with tailored functional properties. The opportunity to synthesize these tailored materials motivates the interest in the so-called multiferroics, i.e. materials or composites that simultaneously exhibit ferroelectricity (FE) and ferromagnetism (FM) or antiferromagnetism (AF).[1] Specifically, the class of perovskite oxides (ABO_3) has garnered much attention due to the possibility of creating epitaxial superlattices composed of stacks of alternating sublayers, each with their own order parameter, formed with atomic-scale control, and designed to exploit interactions at interfaces. [2-5] A few remarkable examples have shown the appearance of an additional order parameter (i.e. superconductivity or ferromagnetism) at interfaces despite the fact that it does not exist in the constituent materials.[6-8] Epitaxial layers interact via strain, electrostatic, and magnetic effects, all of which are highly sensitive to atomic-scale features. For example, the spins within the surface layer of a G-type AF such as $La_{1-x}Sr_xFeO_3$ are compensated, and exchange interactions are predicted to occur via the spin-flop mechanism [6, 7]. We have recently confirmed this prediction in superlattices consisting of alternating six unit cell thick $La_{0.7}Sr_{0.3}MnO_3$ (LSMO) and $La_{0.7}Sr_{0.3}FeO_3$ (LSFO) layers [8]. In the present study, we show that the AF and FM properties in this superlattice system exhibit dissimilar dependencies on temperature and sublayer thickness and we identify the importance of short-range electronic effects (i.e. charge transfer), in addition to long range (dipole) interactions and magnetic anisotropy. Furthermore, we find that the

magnetic-field induced reorientation of the AF spin axis via the spin-flop mechanism is possible only in a narrow range of sublayer thickness. These results illustrate the importance of the delicate balance between exchange coupling, electronic reconstruction, and long-range interactions in these interfacial phenomena.

LSMO exhibits colossal magnetoresistance, a high degree of spin polarization, a Curie temperature above room temperature (T_C ~ 360 K),[9] as well as coincident FM/paramagnetic and metal/insulator transitions mediated by the Mn^{4+} - O^{2-} - M^{3+} double exchange mechanism.[10] The replacement of Mn with Fe leads to an AF insulator state in $La_{0.7}Sr_{0.3}FeO_3$ (LSFO) with a Néel temperature, T_N ~ 360 K,[11, 12] similar to the T_C of LSMO for the same Sr/La ratio. In this work, LSMO and LSFO epitaxial films and superlattices were grown on (001)-oriented single crystal $SrTiO_3$ (STO) substrates by pulsed laser deposition using a KrF laser (248 nm) at 10 Hz, a fluence ~1.2 J/cm^2, a substrate temperature of 700°C and an oxygen pressure of 200 mTorr. *In situ* reflection high energy electron diffraction monitored the growth rate and verified the layer-by-layer growth mode. After deposition, the superlattices were cooled slowly to room temperature in an oxygen pressure of ~300 Torr to ensure the proper oxygenation of the films. The notation for the superlattices consists of the following: [*# unit cells LSFO* x *# unit cells LSMO*] *# of repeats*. In all cases, the LSMO layer was grown first, so that the LSFO layer lies at the surface of the superlattice. The uniform doping level across both films prevents Sr diffusion between layers. For comparison, single layer films with ~40 nm thickness of LSMO, LSFO, and the LSFO/LSMO solid solution (i.e. $La_{0.67}Sr_{0.33}Fe_{0.5}Mn_{0.5}O_3$) were also grown.

Atomic force microscopy shows an exceptionally low rms roughness below 0.5 nm, irrespective of the superlattice period. The structural properties of the films were measured by

x-ray reflectivity and high-resolution x-ray diffraction (XRD) using a Bruker D8 Discover four-circle diffraction system and beamlines 2-1 and 7-2 at the Stanford Synchrotron Radiation Laboratory (SSRL). Satellite peaks and thickness fringes are observed for the superlattices in the *l* scans of the out-of-plane 002 reflection, attesting to the smooth interfaces and permitting us to accurately confirm the periodicity of the superlattice structures. In thin film form, rhombohedral LSMO can be described using its pseudo-cubic lattice (a = 3.87 Å), so that the film shares the same crystallographic indices as the cubic STO substrate (a = 3.905 Å). Different pseudo-cube-on-cube epitaxial relationships between bulk LSFO and STO are possible; however, the structure of the LSFO films studied here is tetragonal ($a = b \neq c$, with $\boldsymbol{c}$ normal to the substrate surface) within experimental resolution. Reciprocal space maps around the 103, 301, and 331 reflections demonstrate that all superlattices are fully strained to the STO substrate, resulting in the same tetragonal distortion of the LSMO and LSFO layers independent of the sublayer thickness. The full widths at half maximum (FWHM) of the film ω scans for the superlattices (0.024° to 0.028°) and the solid solution (0.039°) were only slightly higher than the typical value of ~0.013° for the substrate, again confirming the high degree of crystallinity.

The macroscopic magnetization was measured using a Quantum Design superconducting quantum interference device (SQUID) magnetometer, with the magnetic field applied in the plane of the film either along the <100> or <110> substrate directions. Its temperature dependence (Fig. 1) was measured for the LSMO film, the superlattices, and the solid solution film with an applied magnetic field, H_a = 100 Oe. The magnetization is normalized to the thickness of the LSMO layers only. The LSMO film exhibits a bulk-like T_C ~ 340 K and a saturation magnetization, M_s ~ 600 emu/cm^3 (3.8 μ_B/Mn) at 10 K. No appreciable magnetization

is observed for the solid solution film in agreement with results for Fe-doped LSMO.[13-15] With decreasing sublayer thickness, the values of T_C and M_s decrease, reaching 300 K and ~150 - 200 K, and 232 emu/cm^3 and 90 emu/cm^3, for [18x18]5 and [6x6]10, respectively. Finally, the magnetization of [3x3]75 approaches that of the solid solution film. This trend of reduced T_C and M_s agrees with reports for ultra-thin LSMO films below ~20 unit cells.[16-20] Hysteresis loops show that the easy magnetization direction for all superlattices lies along the <110> direction, in agreement with published results for LSMO films grown on (001)-oriented STO substrates as a consequence of the 0.64% tensile strain imposed from the substrate.[21] The coercive field for [18x18]5 at 10 K is ~480 Oe, only slightly higher than that of a single layer of LSMO on STO. However, the coercive field increases to ~1700 Oe for [6x6]10, indicating that the magnetization reversal in the LSMO layer is influenced by the exchange coupling to the adjacent LSFO layer at small sublayer thicknesses, as discussed below.

Magnetotransport properties as a function of temperature (Fig. 2) were measured using the van der Pauw geometry with H_a = 0 and 5 T applied along the in-plane <100> direction. The resistivity, ρ, of each superlattice is calculated from its resistance using the simplified assumption that the entire stack rather than only the lower-resistivity LSMO layers contribute to the conduction. Mirroring the magnetization data, the superlattices' $\rho(T)$ behavior approaches that of the solid solution film with decreasing period. A well-defined metal-insulator transition at T_C is observed only in the LSMO film and the [18x18]5 superlattice and it is accompanied by a negative peak in the magnetoresistance, $MR = [\rho(H = 5T) - \rho(H = 0T)]/\rho(H = 0T)$. While already in [18x18]5, the T_C is depressed by 40K and the resistivity increased by an order of magnitude across the entire temperature range, the

behavior of these thicker LSMO sublayers differs fundamentally from that of the [3x3]10 superlattice and the solid solution film. These samples display insulating behavior across the entire temperature range and no *MR*. This trend in the magnetotransport properties with decreasing thickness agrees with previous reports for ultra-thin LSMO films.[17-19] At the intermediate period, [6x6]10 exhibits insulating characteristics with a large negative *MR* which monotonically increases in magnitude with decreasing temperature. As with the magnetization data, the large magnitude of the *MR* observed in [6x6]10 appears to be related to the exchange coupling between the adjacent LSFO and LSMO layers.

X -ray magnetic circular and linear dichroism (XMCD/XMLD) experiments were performed at beamlines 4.0.2 and 6.3.1 of the Advanced Light Source[22] in order to probe the near surface FM/AF properties of the superlattices with element specificity. XMCD spectra were obtained at 30° grazing incidence in applied field, H_a = +/- 0.27 T parallel to the x-ray beam. The Mn XMCD data (not shown) exhibit the same sublayer thickness dependence as the SQUID data, i.e. a decreasing magnetization with decreasing sublayer thickness. This result demonstrates the magnetic uniformity of the superlattice stacks, allowing us to conclude that near surface x-ray absorption (XA) data is representative of the entire superlattice.

In bulk LSFO (Pbnm, a = 5.501 Å, b = 5.544 Å, and c = 7.846 Å),[23] the AF axis, $\boldsymbol{M}_{Fe}$, lies along the ***a***-axis.[24] Studies of $LaFeO_3$ thin films[25, 26] show that the direction of $\boldsymbol{M}_{Fe}$ differs compared to the bulk and is sensitive to the growth method and the strain state. Therefore, to analyze the change of $\boldsymbol{M}_{Fe}$ in our superlattices with sublayer thickness, we reference its orientation to that found in our LSFO films. The AF order in LSFO was probed through Fe $L_{3,2}$ XMLD spectra obtained in grazing-incidence with H_a = 0 and the x-rays impinging at 30° with

respect to the sample surface. The x-ray polarization, $\boldsymbol{E}$, is applied either in-plane (along the [010] substrate direction) or at 60° with respect to the sample surface (referred to as out-of-plane [001] substrate direction) and thereby providing information on the orientation of $\boldsymbol{M}_{Fe}$ with respect to the sample surface.

At 50 K, the Fe XMLD spectra (Fig. 3) for all superlattices are nearly identical whereas the sign of the XMLD is reversed for the solid solution and LSFO films (not shown). To interpret these spectra, we first note that the Fe^{3+} ions in LSFO are surrounded by O^{2-} ions in an octahedral symmetry, similar to that of the Fe^{3+} on the B site in the spinel Fe_3O_4. Therefore, we employ the analysis of XMLD spectra as described in Ref. [27], which indicates an in-plane alignment of $\boldsymbol{M}_{Fe}$ in the superlattices and conversely an out-of-plane canting for the solid solution and LSFO films. These equally-strained solid solution and LSFO films are used as "end-member" reference points, allowing us to conclude that the AF properties of the superlattices do not approach those of the end-members, contrary to the case of the FM behavior of the same superlattices. The AF signature remains in [6x6]10 and [18x8]5 beyond room temperature but disappears for [3x3]10 and the solid solution film between 150 K and room temperature. Even without a full investigation of the temperature dependence of T_N, we clearly observe a gradual trend of decreasing T_N with decreasing sublayer thickness. This decrease occurs much more slowly than the observed decrease in the T_C of the LSMO layers, such that even at three unit cell thickness, the LSFO layer remains in an AF state. Comparatively fewer studies have been performed on the thickness dependence of AF properties, particularly for the perovskite oxides, though reports on NiO have shown a rapid decrease in T_N between five and 10 unit cell film thickness.[28] In addition, the 2-D nature of the superlattice structure

confines $\boldsymbol{M}_{Fe}$ to lay in-the-plane of the sample. Therefore, T_N and the direction of $\boldsymbol{M}_{Fe}$ in this superlattice structure exhibit fundamentally different dependencies on the sublayer thickness than their FM counterparts.

In order to further explore the differing thickness dependence of the FM and AF properties of the superlattices, the XA spectra for the Mn $L_{3,2}$ absorption edges of the samples are shown in Figure 4. The solid solution film and [3x3]10 display a slight shift of the main L_3 peak to higher photon energy as well as the presence of an additional peak about 2 eV below the main L_3 peak. These signatures have been ascribed to an increased concentration of Mn^{4+} ions.[29, 30] Due to the uniform Sr doping level, the change in the Mn^{3+}/Mn^{4+} ratio is not expected to be related to A-site chemical doping effects. Alternatively, a charge transfer involving an electron transferring from the LSMO layers to LSFO layers ($Mn^{3+} \rightarrow Mn^{4+}$) across the interface as proposed by Kumigashira and coworkers [31] might be expected. The ground state of the LSFO system for small Sr doping (x<0.5) is the Fe^{3+} - ligand hole state.[29] In accordance, the electrons involved in the charge transfer go to states of primarily oxygen character and no significant difference is observed in the Fe XA spectra for any sample. Characteristic length scales over which such charge transfer mechanisms occur have been determined in other perovskite systems, such as $SrTiO_3/LaTiO_3$ [32] and $LaMnO_3/SrMnO_3$ [33] and typically range in the order of a few unit cells, consistent with our observations. The interfacially-induced valence changes effectively push the LSMO system towards the case of *higher* Sr doping (yielding a FM metal with *decreased* T_C). Therefore, together with the decrease in long-range (dipole) interactions due to finite size effects, this mechanism clearly contribute to the rapid decrease of T_C and M_s with decreasing sublayer thickness, i.e. the magnetization and

magnetotransport properties trend from those of LSMO film towards the solid solution film. For the LSFO sublayers, the Fe valence state is nearly unchanged by the charge transfer, and consequently the T_N is only weakly dependent on sublayer thickness. The observed gradual decrease in T_N is likely due to the decrease in magnetic anisotropy with decreasing sublayer thickness. Additional effects (such as interfacial stabilization of oxygen vacancies within LSFO even in strong oxidizing conditions) cannot be ruled out. These results illustrate the complexity of the effects observed at interfaces and the importance of determining the properties on the length scale of a few unit cells.

An additional XMLD measurement allows us to investigate the coupling between the LSFO and LSMO layers in the superlattices. These measurements (discussed in detail elsewhere[8]) are taken in a normal incidence geometry with H_a = 0.3 T parallel or perpendicular to the x-ray $\boldsymbol{E}$ vector. This magnetic field is sufficient to align the Mn moments in any direction within the surface plane. Any coupling between the LSFO and LSMO layers will result in an observable change in the Fe $L_{3,2}$ XA spectra. The solid solution film and [3x3]10 show no FM order and as expected, no coupling is observed. In contrast, for [6x6]10 we find a robust orthogonal coupling between the LSFO and LSMO layers, imposing an orientation of $\boldsymbol{M}_{Fe}$ such that it lies within the film plane but at 90° with respect to the in-plane Mn moments regardless of their direction within the plane. This result agrees with predictions from a microscopic Heisenberg model[6, 7, 34] for the (001)-surface of a G-type AF such as LSFO, where an equal number of positive and negative exchange interactions exist. The large coercive field observed in the magnetization data for this sample confirms the importance of the exchange coupling. Upon further increase in the sublayer thickness to [18x18]5, the XMLD decreases to near zero:

the magnetic anisotropy in the LSFO layers now dominates. Thus, exchange coupling at this thickness plays a comparatively weaker role, and the coercive field correspondingly returns to a value near that of the LSMO film.

In summary, we have characterized a series of all-perovskite oxide superlattice structures consisting of AF LSFO layers and FM LSMO layers – two materials which exhibit nearly equal critical temperatures in the bulk. The two order parameters display dissimilar behavior with decreasing temperature and sublayer thickness. For LSFO, the 2-D confinement preserves an in-plane orientation of the AF axis and leads to a gradual decrease in magnetic anisotropy and T_N, while for LSMO, the FM properties trend towards the solid solution due to the combined effects of a charge transfer at the LSFO interfaces and diminished long-range interactions. In addition, using soft x-ray magnetic dichroism, we observe that an applied magnetic field reorients the AF axis in LSFO via spin-flop coupling to the LSMO layers only in a small range of sublayer thickness. Understanding the competition between these interactions (exchange, interfacial electronic reconstruction, and long-range interactions) provides a promising means to separately control the FM and AF properties in superlattice structures, independent of strain or chemical effects.

The authors would like to thank Dr. A. Mehta and M. Bibee for assistance in acquiring the XRD data at SSRL, and Dr. R. Chopdekar and Prof. Y. Suzuki (UC Berkeley) for assistance with the magnetotransport measurements. Research at the ALS, CNMS, and SSRL is supported by the Division of Scientific User Facilities, Office of Basic Energy Sciences, U.S. Department of Energy. Research at UC Davis is supported by UC Davis start-up funds and the National Science Foundation CAREER Award DMR 0747896 (Y.T.).

Figure Captions:

Figure 1: (Color online) Magnetization as a function of temperature for the superlattices, solid solution film, and LSMO film with H_a=100 Oe.

Figure 2: (Color online) (a) Resistivity and (b) magnetoresistance as a function of temperature for the superlattices, solid solution film, and LSMO film.

Figure 3: (Color online) (a) XA spectra for the [6x6]10 superlattice with ***E*** // [001] (black curve) and ***E*** // [010] (red curve), and (b) XMLD spectra defined as ***E*** // [010] – ***E*** // [001] for the superlattices and the solid solution film. All the superlattices possess the same characteristics which are *opposite* to that of the solid solution film and the LSFO film (not shown).

Figure 4: (Color online) Mn XA spectra for the superlattices, the solid solution film, and LSMO film. An additional feature 2 eV below the main Mn L_3 peak appears as the sublayer thickness decreases.

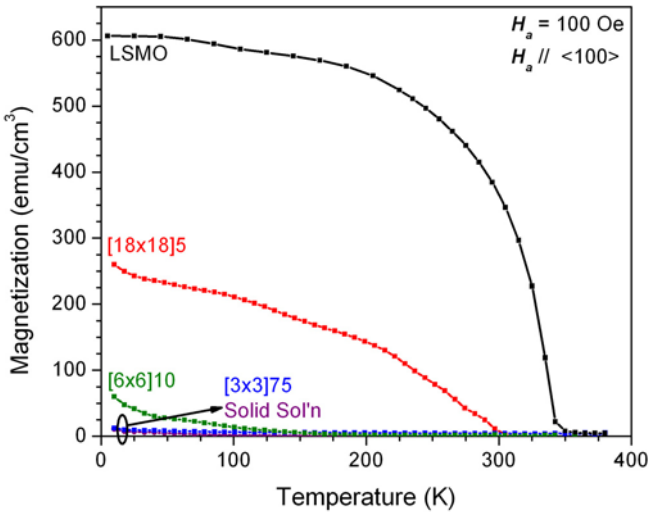
H_a = 100 Oe
H_a // <100>
LSMO
[18x18]5
[6x6]10
[3x3]75
Solid Sol'n
Magnetization (emu/cm^3)
Temperature (K)
0
100
200
300
400
500
600

Figure 1

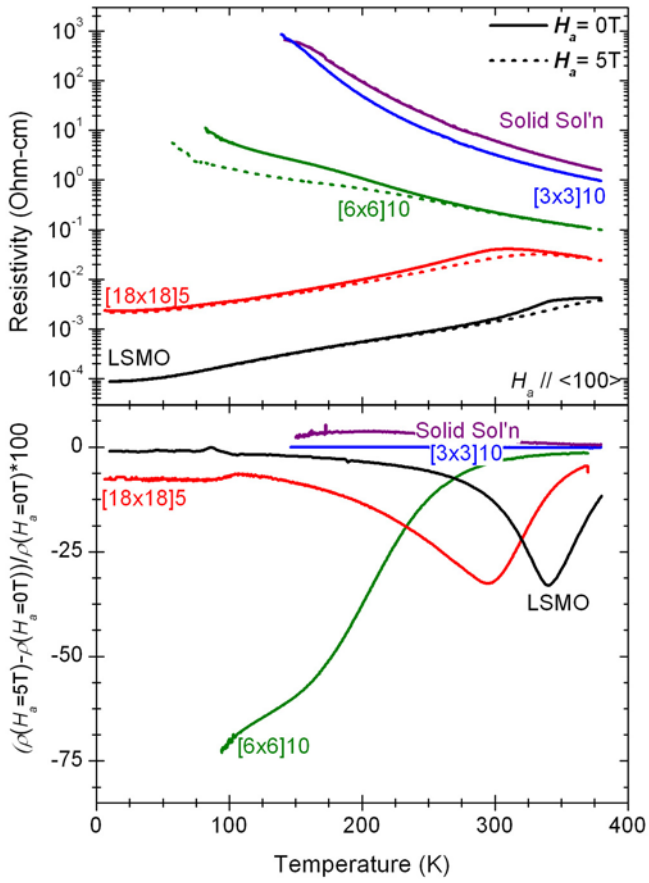
H_a = 0T
H_a = 5T
Solid Sol'n
[3x3]10
[6x6]10
[18x18]5
LSMO
H_a // <100>
Resistivity (Ohm-cm)
10^3
10^2
10^1
10^0
10^{-1}
10^{-2}
10^{-3}
10^{-4}
$(\rho(H_a=5T)-\rho(H_a=0T))/\rho(H_a=0T)*100$
0
-25
-50
-75
0
100
200
300
400
Temperature (K)

Figure 2

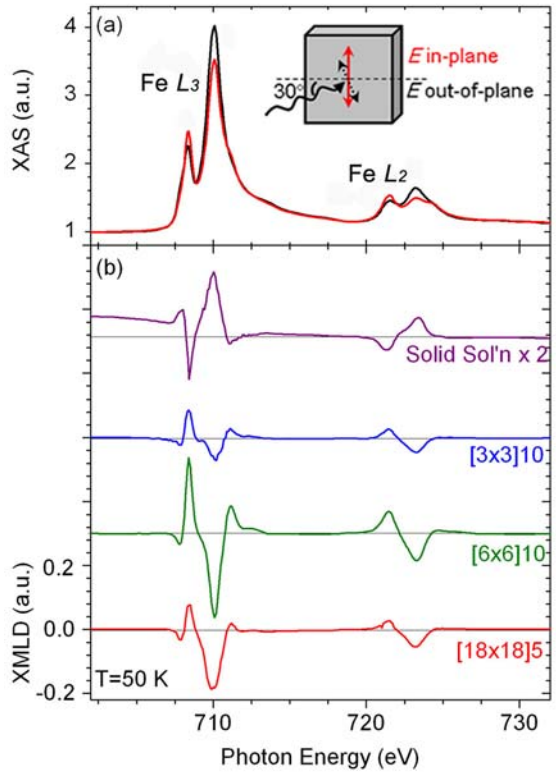
(a)
Fe L_3
Fe L_2
E in-plane
E out-of-plane
30°
XAS (a.u.)
4
3
2
1
(b)
Solid Sol'n x 2
[3x3]10
[6x6]10
[18x18]5
T=50 K
XMLD (a.u.)
0.2
0.0
-0.2
710
720
730
Photon Energy (eV)

Figure 3

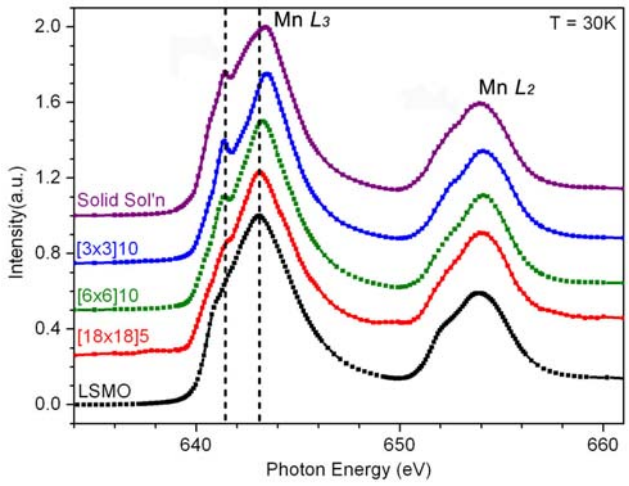
Mn L3
T = 30K
Mn L2
Solid Sol'n
[3x3]10
[6x6]10
[18x18]5
LSMO
Intensity(a.u.)
Photon Energy (eV)
2.0
1.6
1.2
0.8
0.4
0.0
640
650
660

Figure 4

References

[1] R. Ramesh, and N. A. Spaldin, Nat. Mater. **6**, 21 (2006).

[2] H. Yamada *et al.*, Science **305**, 646 (2004).

[3] D. G. Schlom *et al.*, J. Am. Ceram. Soc. **91**, 2429 (2008).

[4] H. N. Lee *et al.*, Nature **433**, 395 (2005).

[5] H. M. Christen, D. H. Kim, and C. M. Rouleau, Applied Physics A **93**, 807 (2008).

[6] L. L. Hinchey, and D. L. Mills, Phys. Rev. B **34**, 1689 (1986).

[7] N. C. Koon, Phys. Rev. Lett. **78**, 4865 (1997).

[8] E. Arenholz *et al.*, Appl. Phys. Lett. **94**, 072503 (2008).

[9] A. P. Ramirez, J. Phys-Condens Mat **9**, 8171 (1997).

[10] P.-G. de Gennes, Phys. Rev. **118**, 141 (1960).

[11] J.-C. Grenier *et al.*, Mater. Res. Bull. **19**, 1301 (1984).

[12] U. Shimony, and J. M. Knudsen, Phys. Rev. **144**, 361 (1966).

[13] K. H. Ahn *et al.*, Phys. Rev. B **54**, 15299 (1996).

[14] J. Dho, and N. H. Hur, Solid State Communications **138**, 152 (2006).

[15] A. Tiwari, and K. P. Rajeev, J. Appl. Phys. **86**, 5175 (1999).

[16] C. A. F. Vaz, J. A. C. Bland, and G. Lauhoff, Rep. Prog. Phys. **71**, 056501 (2008).

[17] M. Huijben *et al.*, Phys. Rev. B **78**, 094413 (2008).

[18] R. V. Chopdekar, E. Arenholz, and Y. Suzuki, Phys. Rev. B **79**, 104417 (2009).

[19] J. Z. Sun *et al.*, Appl. Phys. Lett. **74**, 3017 (1999).

[20] A. Tebano *et al.*, Phys. Rev. Lett. **100**, 137401 (2008).

[21] L. M. Berndt, V. Balbarin, and Y. Suzuki, Appl. Phys. Lett. **77**, 2903 (2000).

[22] E. Arenholz, and S. O. Prestemon, Rev. Sci. Instrum. **76**, 183908 (2005).

[23] in *Powder Diffraction File #01-089-1269* (International Centre for Diffraction Data.

[24] R. L. White, J. Appl. Phys. **40**, 1061 (1969).

[25] J. Luning *et al.*, Phys. Rev. B **67**, 214433 (2003).

[26] S. Czekaj *et al.*, Phys. Rev. B **73**, 020401(R) (2006).

[27] E. Arenholz *et al.*, Phys. Rev. B **74**, 094407 (2006).

[28] D. Alders *et al.*, Phys. Rev. B **57**, 11623 (1998).

[29] M. Abbate *et al.*, Phys. Rev. B **46**, 4511 (1992).

[30] F. M. F. de Groot, J. Electron Spectrosc **67**, 529 (1994).

[31] H. Kumigashira *et al.*, Appl. Phys. Lett. **84**, 5353 (2004).

[32] A. Ohtomo *et al.*, Nature **419**, 378 (2002).

[33] S. Smadici *et al.*, Phys. Rev. Lett. **99**, 196404 (2007).

[34] T. C. Schulthess, and W. H. Butler, Phys. Rev. Lett. **81**, 4516 (1998).